NORSAR

ROYAL NORWEGIAN COUNCIL FOR SCIENTIFIC AND INDUSTRIAL RESEARCH

Scientific Report No. 5-74/75

FINAL TECHNICAL REPORT
NORSAR PHASE 3

1 July 1974 – 30 June 1975

Prepared by
K. A. Berteussen

Kjeller, 8. August 1975

Sponsored by
Advanced Research Projects Agency
ARPA Order No. 2551

APPROVED FOR PUBLIC RELEASE, DISTRIBUTION UNLIMITED

E. THE EFFECT OF ARRAY CONFIGURATION ON SLOWNESS AND AZIMUTH ANOMALIES

The multitude of sensors characterizing the large seismic arrays makes it possible to test what effect a change in array configuration has on the slowness and azimuth anomalies for P-phases recorded at the arrays. In two recent papers this effect has been studied both for LASA (Berteussen, 1975a) and NORSAR (Berteussen, 1975b).

On Fig. E.1 the 'array diagram' for a set of well-recorded P-phases at LASA using all 21 subarrays is shown. The tail of the arrows represents the slowness and azimuth ($dT/d\Delta$, Φ) estimated at the array, while the head represents the values entailed by a (laterally homogeneous) standard earth model. On Fig. E.2 the same array diagram is then shown when only odd numbered LASA subarrays have been used. The configuration is somewhat 'thinner' than the full array, but has approximately the same aperture (200 km). Comparing Figs. E.1 and E.2, it is immediately apparent that certain sectors (especially azimuth $90^{\circ} \lesssim \Phi \leq 270^{\circ}$) of the two array diagrams are significantly different. In particular, the anomalies associated with rays which bottom in the vicinity of proposed plume structures under Hawaii ($\Phi \sim 265^{\circ}$) at LASA and the Galapagos Islands ($\Phi \sim 155^{\circ}$) (Davies and Sheppard, 1972, Kanasewich et al, 1973) are markedly different in the two figures. Anomalies associated with rays bottoming in the lowest mantle beneath Iceland ($\Phi \sim 20^{\circ}$) are essentially consistent on Figs. E.1 and E.2; however, array diagrams for other configurations (Berteussen, 1975a) demonstrate conclusively that these anomalies are also critically dependent on the spatial sampling of the wavefront.

The same effects may also be demonstrated at NORSAR. On Fig. E.3 the array diagram for the full NORSAR array is shown, while Fig. E.4 shows a diagram using subarrays 1, 5-8, 15-20, giving us an array of aperture 70 km instead of the 100 km aperture of the whole NORSAR. For the azimuth section

330-120 degrees it is seen that the vectors have been rotated by almost 90 degrees relative to those on Fig. E.3. Also note that for azimuth 300 degrees (the direction to Iceland) Fig. E.4 shows rapid variations in the anomaly pattern. Given a NORSAR array consisting of only these eleven sub-arrays, one could, following Davies and Sheppard (1972) and Kanasewich et al (1973), be tempted to associate these rapid changes with, for example, a hot spot under Iceland. However, a more complete picture (Fig. E.3) demonstrates that such an interpretation would be erroneous. Using smaller arrays and fewer subarrays even more drastic variations can of course be induced. On Fig. E.5 the array diagram for the NORSAR subarray combination 2, 3, 9, 10, 11, giving an aperture of some 45 km, which still is larger than most of the medium-sized arrays, is shown. For the direction towards Iceland, the arrows are now seen to be turned quite opposite to those on Fig. E.4. Also for the rest of the slowness-space large differences are observed relative to the data on Figs. E.3 and E.4. Finally, (Fig. E.6) an array diagram is shown using only the subarrays 6, 17, 20. This configuration is approximately the same as that of the Hagfors array in Sweden, and demonstrates that for such a small array almost 'any' type of location errors may be found. On Fig. E.6 one interesting detail should be noted. One of the arrows (azimuth~0) is seen to be turned in almost the same direction as the core phases between azimuth 0° and 90°, and directly opposite to the surrounding P-wave vectors, thus indicating that the anomaly for the core phases is a function only of direction of approach of the ray.

Clearly, there are a lot of details in each of these figures which it would be tempting to associate with structures far away from the receiver. The fact that these details are not retained as one changes configuration suggests, however, that in reality the wavefronts are locally delayed or speeded up for example by rapid Moho depth variations and/or scattering by small-scale randomly distributed inhomogeneities close

to the receiver. The final estimates of slowness and azimuth are then very much dependent on which sites are sampled and which are not. Of course, source side or deep mantle effects may be present in the data, but local structural effects have been shown to be so dominant and so difficult to characterize (and therefore to correct for) that there can be no justification for speculating on structures well removed from the array on the basis of these data.

K.A. Berteussen

REFERENCES

Berteussen, K.A. (1975a): Array analysis of lateral inhomogeneities in the deep mantle, submitted for publication.

Berteussen, K.A. (1975b): The origin of slowness and azimuth anomalies at large arrays, submitted for publication.

Davies, K., and R.M. Sheppard (1972): Lateral heterogeneity in the earth's mantle, Nature, 239, 318-323.

Kanasewich, E.R., R.M. Ellis, C.H. Chapman, P.R. Gutowski (1973): Seismic array evidence of a core-boundary source for the Hawaiian linear volcanic chain, J. Geophys. Res., 78, 1361-1371.

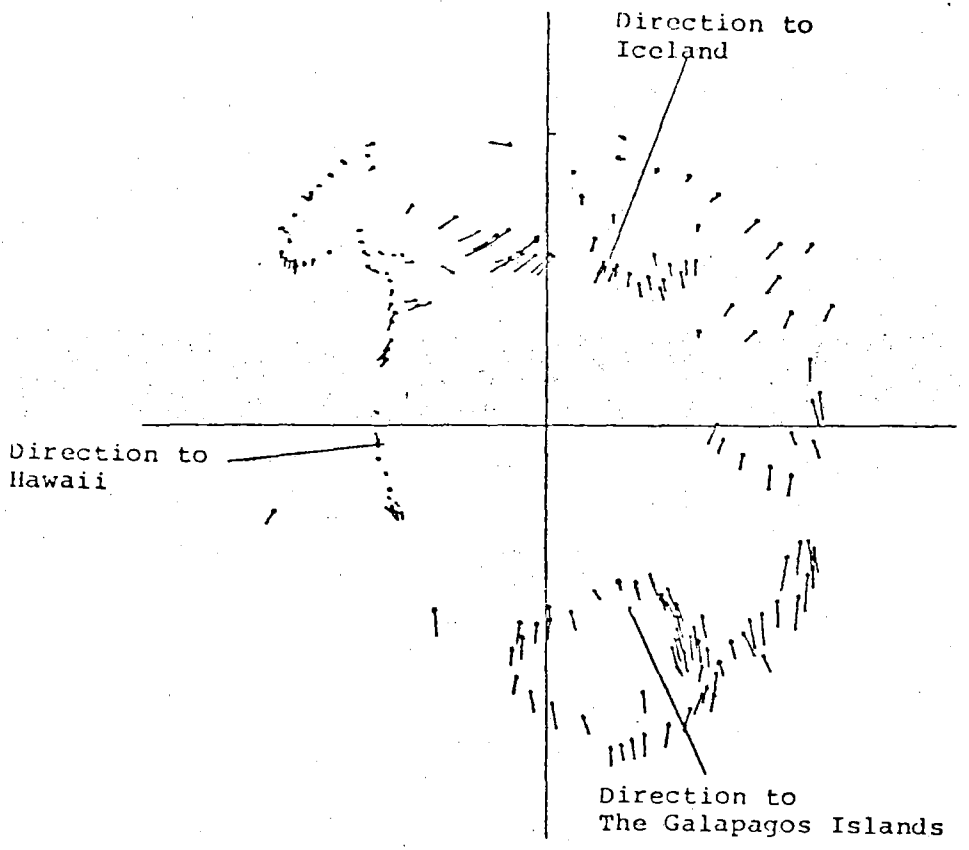

Fig. E.1 Array diagram for a configuration consisting of all 21 LASA subarrays. The tail of the arrows represents the observed ($dT/d\Delta$, Φ), i.e., the slowness-space location measured at LASA. The head of the arrows represents the ($dT/d\Delta$, Φ) one expects using the PDE event location and standard distance-slowness tables.

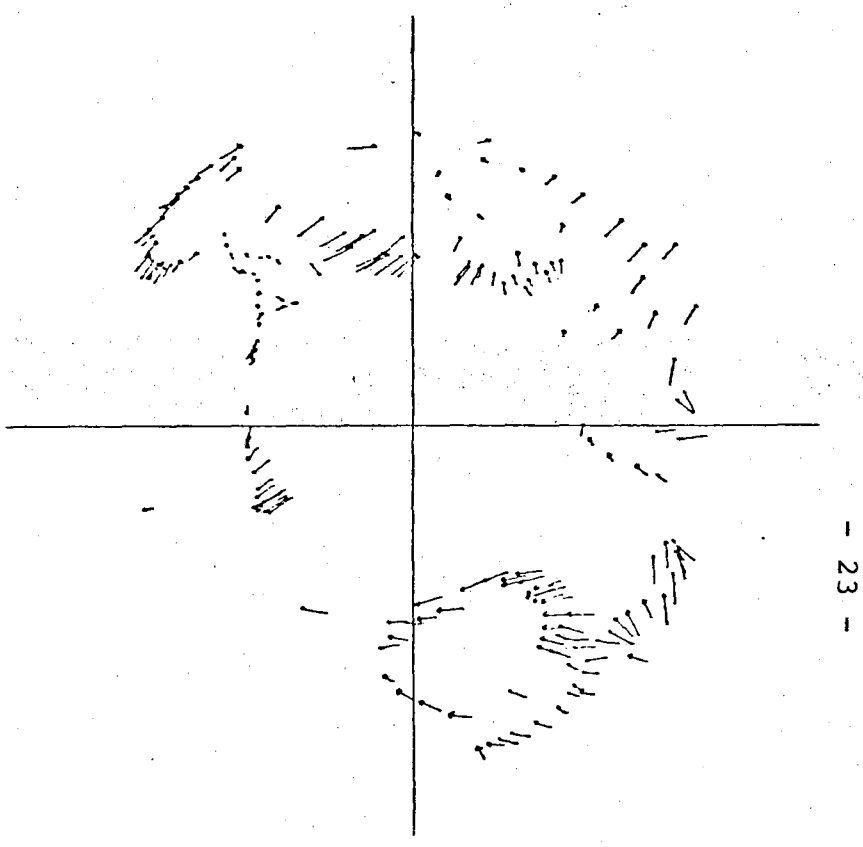

Fig. E.2 Same as Fig. E.1 for the LASA subarrays 1,3,5,7,9,11,13,15,17,19,21 (A0,B2,B4,C2,C4,D2,D4,E2,E4,F2,F4).

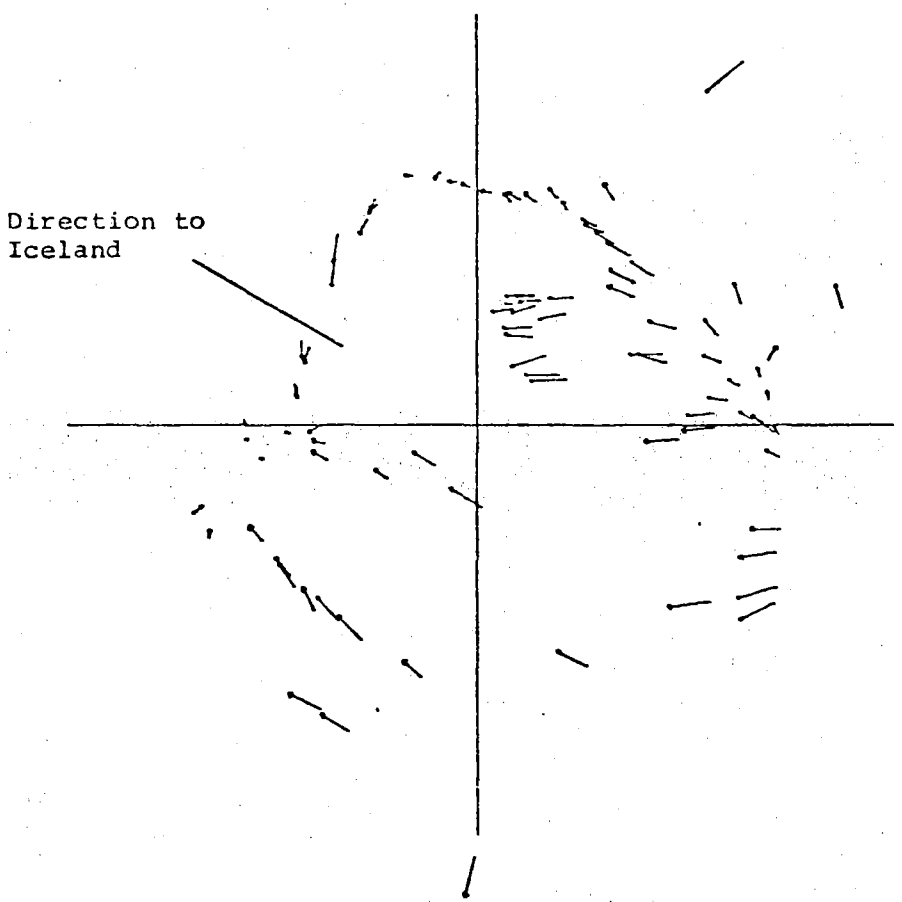

Fig. E.3 Same as Fig. E.1 for all 22 NORSAR subarrays.

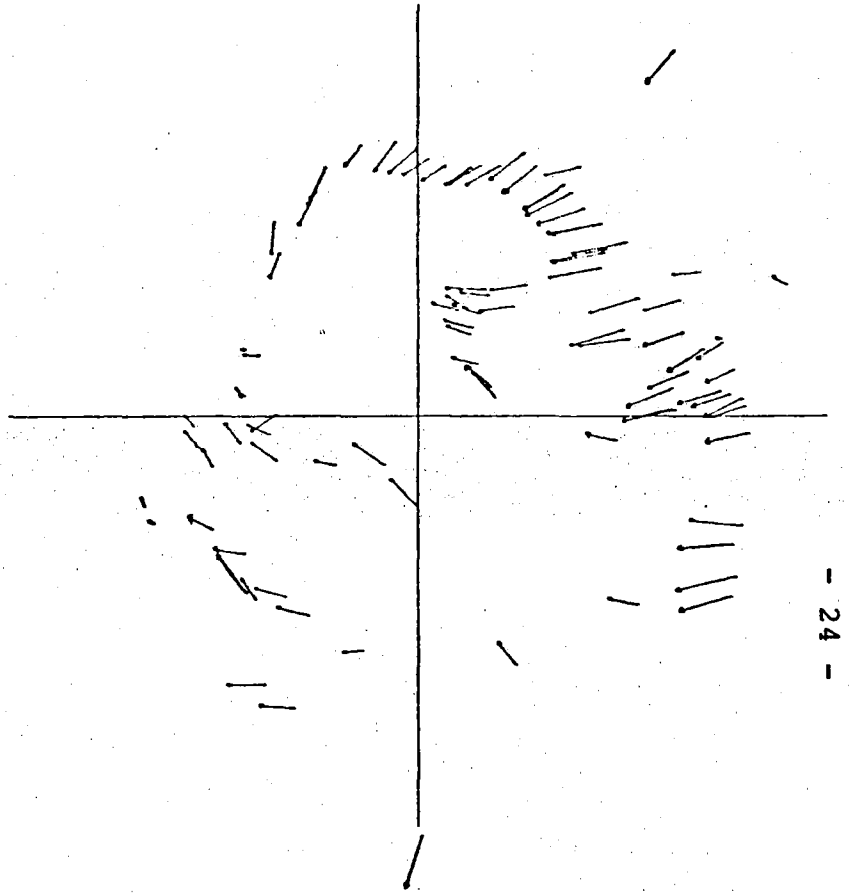

Fig. E.4 Same as Fig. E.1 for the NORSAR subarrays 1, 5-8, 15-20 (1A, 4B-7B, 7C-12C).

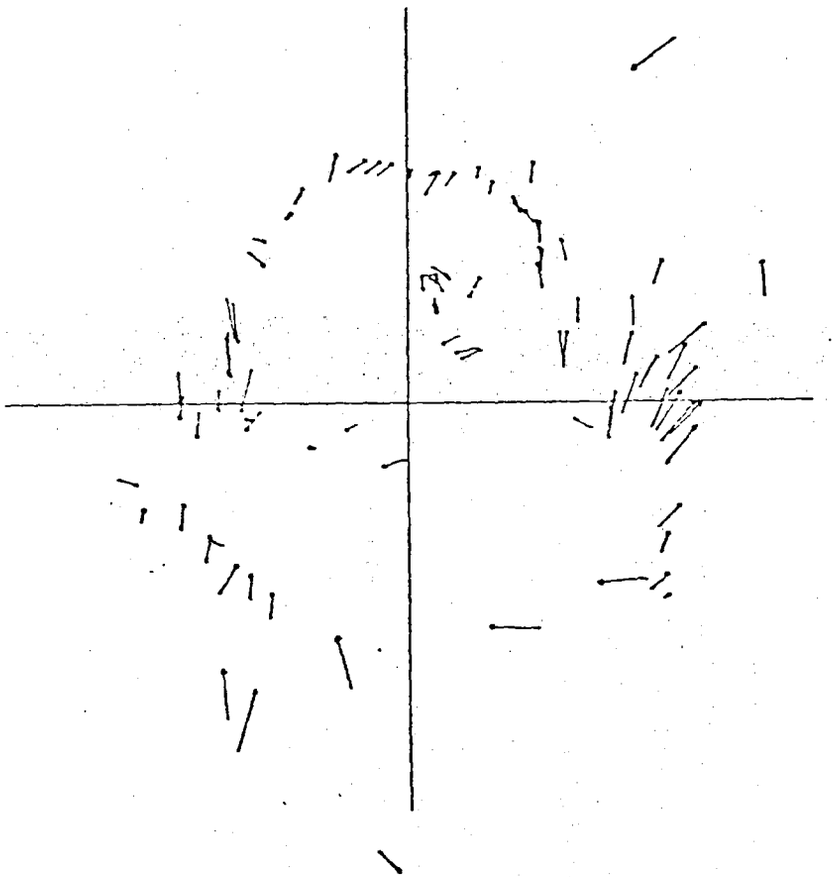

Fig. E.5 Same as Fig. E.1 for the NORSAR subarrays 2,3,9,10,11 (1B,2B,1C,2C,3C).

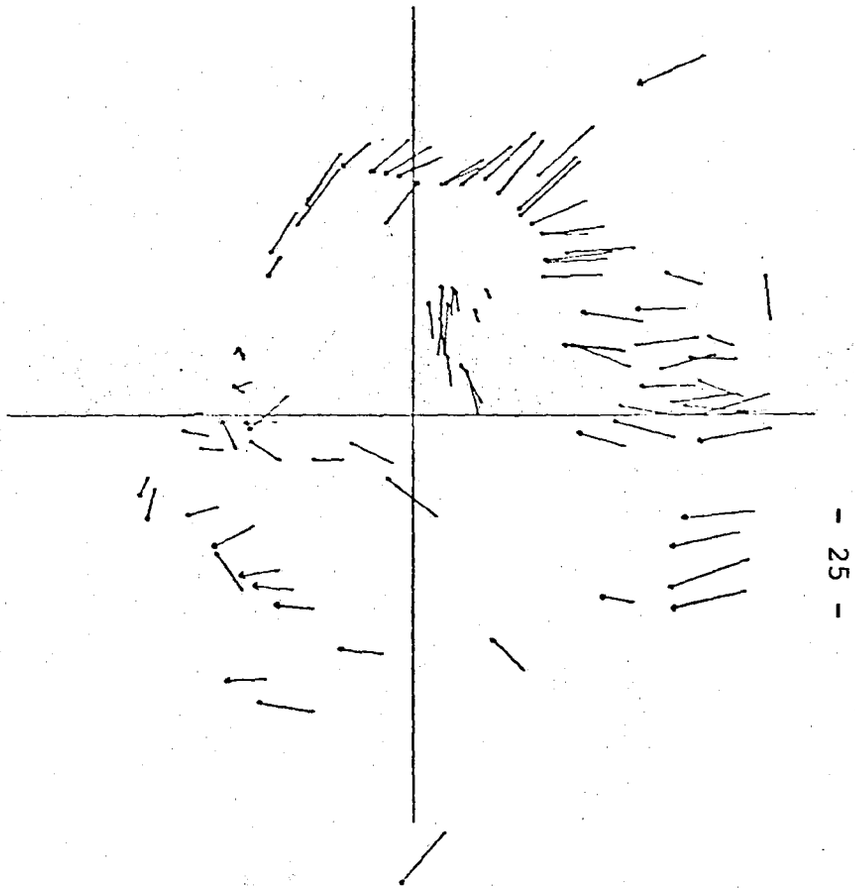

Fig. E.6 Same as Fig. E.1 for the NORSAR subarrays 6, 17, 20 (5B, 9C,12C).